AMORPHOUS ANALOGS OF MARTIAN GLOBAL SOIL: PAIR DISTRIBUTION FUNCTION ANALYSES AND IMPLICATIONS FOR SCATTERING MODELS OF CHEMIN X-RAY DIFFRACTION DATA. C. N. Achilles[1], D. L. Bish[1], E. B. Rampe[2], R. V. Morris[3] [1]achillec@indiana.edu, Department of Geological Sciences, Indiana University, [2]Aerodyne, Houston, TX, [3]NASA Johnson Space Center, Houston, TX

Introduction: Soils on Mars have been analyzed by the Mars Exploration Rovers (MER) and most recently by the Mars Science Laboratory (MSL) rover. Chemical analyses from a majority of soil samples suggest that there is a relatively uniform global soil composition across much of the planet [1]. A soil site, Rocknest, was sampled by the MSL science payload including the CheMin X-ray diffractometer and the Alpha Particle X-ray Spectrometer (APXS) [2]. CheMin X-ray diffraction (XRD) data revealed crystalline phases and a broad, elevated background, indicating the presence of amorphous or poorly ordered materials (Fig 1). Based on the chemical composition of the bulk soil measured by APXS and the composition of crystalline phases derived from unit-cell parameters determined with CheMin data, the percentages of crystalline and amorphous phases were calculated at 51% and 49%, respectively [3,4].

Attempts to model the amorphous contribution to CheMin XRD patterns were made using amorphous standards and full-pattern fitting methods and show that the broad, elevated background region can be fitted by basaltic glass, allophane, and palagonite [4]. However, the modeling shows only that these phases have scattering patterns similar to that for the soil, not that they represent unique solutions. Here, we use pair distribution function (PDF) analysis to determine the short-range order of amorphous analogs in martian soils and better constrain the amorphous material detected by CheMin.

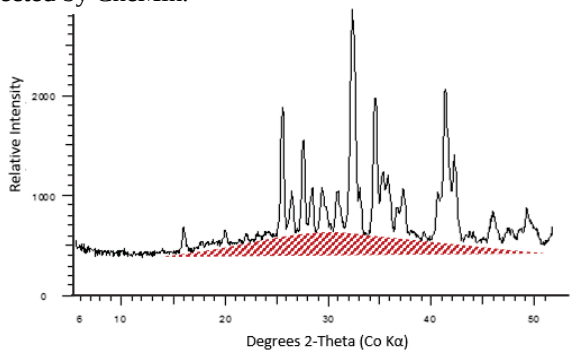

Figure 1. Rocknest CheMin XRD pattern illustrating the intensity contribution due to amorphous scattering (shaded).

Analog Samples and Methods: Analog samples were chosen based on amorphous composition predictions from MER soil analyses and the chemical composition of the Rocknest amorphous component [4,5]. Three glass samples with varying SiO_2 abundance represent basaltic, andesitic, and rhyolitic glass compositions, 48, 60, and 76 wt% SiO_2, respectively. Additionally, a synthetic allophane with a molar Si:Al ratio of 0.7 and a palagonite sample from Hawaii (HWMK-919) were measured.

Laboratory X-ray diffractometers resolve crystalline phases by the positions and intensities of Bragg diffraction peaks, whereas non-Bragg diffuse scattering gives information about deviations from a well-ordered crystal structure. Deviations from crystalline order in nanophase and highly disordered materials produce broad diffuse scattering patterns, elevating the background above the nominal baseline. Each analog sample was analyzed on a Bruker D8 X-ray diffractometer (Cu Kα) to measure the scattering pattern as it would appear in the CheMin XRD instrument. Additionally, samples were measured on the 11-ID-B beamline at the Advanced Photon Source at Argonne National Laboratory to obtain X-ray scattering data (λ = 0.2114Å). The Fourier transform of the total-scattering data, the PDF, allows determination of nearest-neighbor and next-nearest neighbor structural information.

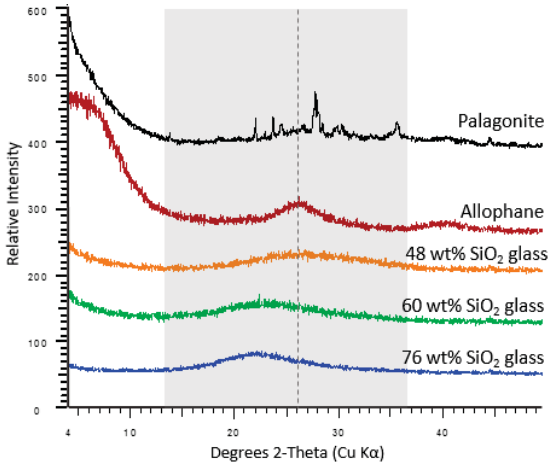

Figure 2. XRD patterns for analog phases. The shaded area illustrates the region and maximum (dashed line) of amorphous scattering in the Rocknest pattern.

Results: Laboratory XRD patterns of amorphous analogs reveal scattering contributions within the same range of *d* as the Rocknest amorphous hump (Fig 2). The composition and short-range structure of each poorly crystalline phase influence the scattering pattern. To explore these relationships, PDF analyses were used to identify subtle changes in atom-atom relationships that correlate to changes in overall structure.

Glasses: A comparison of the three glass samples in Figure 2A illustrates the impact of SiO_2 wt% on the

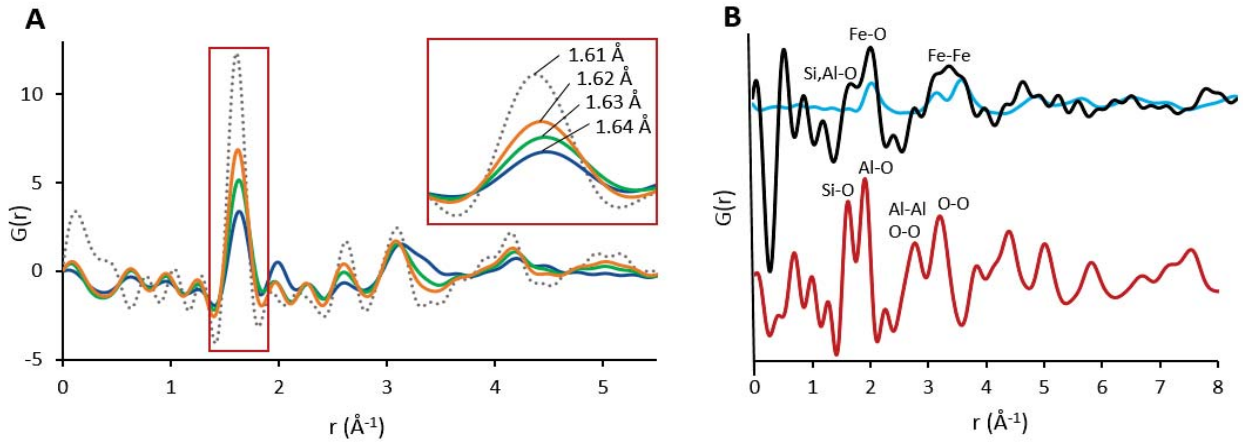

Figure 3. A) PDF of glasses with varying SiO_2 compositions. Dashed ~100 wt%, orange ~48 wt%, green ~60 wt%, and blue ~76 wt% SiO_2. Inset: maxima for the first major peak. B) PDF of palagonite (black), ferrihydrite (blue) and allophane (red).

X-ray scattering data. The most intense peak in the PDF data is located at ~1.61 $Å^{-1}$, the Si-O bond length of tetrahedrally coordinated Si (Fig 2A). As the amount of SiO_2 in the analog material decreases, the amount of tetrahedrally coordinated Al (Al-O bond length ~1.75 $Å^{-1}$) increases, causing the first peak maximum in the PDF to shift to higher values as a function of Si:Al ratio. Although the two peaks (Si-O and Al-O) cannot be individually resolved, calculations confirm that the position of the maximum in the PDF varies with Si:Al ratio. SiO_2 interactions dominate the PDF, although changes in other major elements (e.g., Al, Fe) contribute to the PDF and likely to the overall scattering pattern. Peaks near 2.0 and 3.4 $Å^{-1}$ are likely due to Fe interactions; these relationships will be explored in future models. Scattering patterns for the three glasses (Fig 1) have different maxima in the scattering profiles, shifting to higher 2θ (lower *d*) with decreasing SiO_2.

Allophane and Palagonite: Allophane PDF data are characterized by tetrahedrally coordinated Si and octahedrally coordinated Al as illustrated by peaks at 1.62 and 1.91 $Å^{-1}$, respectively (Fig 2B). Additional peaks in the PDF are attributed to Al-Al and O-O correlations. Palagonite scattering data display contributions from crystalline and amorphous phases (Fig 2B). Feldspar and magnetite comprise the crystalline contribution, and it is predicted that the main amorphous phases are amorphous ferric oxides and/or ferrihydrite [5]. Palagonite PDF data show tetrahedral Si/Al-O correlations at 1.63 $Å^{-1}$, attributed to feldspar, and Fe-O and Fe-Fe correlations likely comprised of a combination of phases. The Fe-O bond length (1.96 $Å^{-1}$) is consistent with octahedrally coordinated ferric iron. Comparison with a synthetic 2-line ferrihydrite shows that the position of the Fe-O and Fe-Fe peaks indicate this phase is likely a component of our palagonite standard. The remaining Fe-O and Fe-Fe amplitudes can be attributed to crystalline magnetite and amorphous ferric oxide phases.

Implications for CheMin Amorphous Modeling: Subtle changes in the short-range order of amorphous phases influence diffuse scattering profiles and can be effectively measured by PDF analyses. Comparing the shape and position of the Rocknest amorphous profile with those from analog samples can provide a first-order determinant of amorphous composition. Basaltic glass, the palagonite amorphous component, and allophane all contain scattering patterns consistent with the maximum position of the Rocknest amorphous profile. The calculated composition of the Rocknest amorphous component contains ~36 wt% SiO_2, ~19 wt% FeO_T, and ~10 wt% SO_3 [3]. The low silica and high iron concentration, combined with the scattering profile, reveal that basaltic glass may be a component of the soil but is not the only amorphous phase present.. Amorphous ferric oxides are compelling candidates for the remaining Fe and palagonite scattering profiles are consistent with the Rocknest profile. Future models will explore additional analogs (e.g. Fe-allophane, sulfates, etc.) and use chemical composition to constrain and estimate the relative contributions of amorphous phases comprising CheMin scattering profiles.

Acknowledgements: This research used resources of the Advanced Photon Source, a U.S. Department of Energy (DOE) Office of Science User Facility operated for the DOE Office of Science by Argonne National Laboratory under Contract No. DE-AC02-06CH11357. Support from the NASA MSL mission is acknowledged, and Dr. James Brophy provided samples and assistance with synthetic glasses.

References: [1] Yen, A.S. et al. (2005) *Nature, 436*. [2] Blake, D.F. et al. (2013) *Science, 341*. [3] Morris, R.V. et al. (2015) *LPS XLVI*. [4] Bish, D.L. et al. (2014) *Science, 341*. [5] Ming, D.W. et al. (2006) *JGR, 111*, E02S12. [5] Morris, R.V. et al. (2001) *JGR, 106* E3, 5057-5083.